ISSN: 3071-186X Volume 01, Issue 03, April, 2026

Scienta Press Journals

American Innovator
Journal of Emerging Technologies and Research

Mathematical Modeling Of Acoustic Cavitation And Sericin Dissolution Kinetics In An Ultrasonic Bath Mechatronic System For Silk Extraction

Botirov Alisher[1], Sharibayev Nosir[2], Rahimov Alisher[3]

[1]Fergana State Technical University, Uzbekistan

[2]Namangan State Technical University, Uzbekistan

[3]Andijan State Technical Institute, Uzbekistan

Abstract

This article presents a comprehensive mathematical model of the physical processes underlying silk extraction from silkworm cocoons in an ultrasonic bath mechatronic system. Three coupled sub-models are developed and integrated: (1) an acoustic cavitation model based on the Rayleigh–Plesset equation describing bubble dynamics in the processing liquid; (2) a sericin dissolution kinetics model formulated as a mass-transfer diffusion problem with ultrasonic enhancement coefficient; and (3) a lumped-parameter thermal model of the bath accounting for heater power input, acoustic energy dissipation, and convective heat loss. The models are validated against experimental data obtained from a prototype mechatronic system operating at 28 kHz. Simulation results show that the combined model predicts sericin softening time within 6.4% of measured values, confirming its suitability for system design optimization and control algorithm development

Keywords: Mathematical modeling, acoustic cavitation, Rayleigh–Plesset equation, sericin dissolution, mass transfer, thermal model, ultrasonic bath, mechatronic system, silk extraction, Bombyx mori.

1. Introduction

The technological effectiveness of ultrasonic silk extraction depends on three tightly coupled physical phenomena: acoustic cavitation in the processing liquid, diffusion-driven dissolution of the sericin protein matrix surrounding cocoon filaments, and the thermal state of the bath medium. While each of these phenomena has been studied independently in the literature [1–4], no unified mathematical framework has been proposed that links all three within the context of a mechatronic reeling system.

Cavitation — the nucleation, growth, and violent collapse of vapor-filled bubbles — is the primary mechanism by which ultrasonic energy is delivered to the sericin–filament interface [3, 10]. The collapse of cavitation bubbles generates localized micro-jets and shock waves with pressures exceeding 100 MPa, disrupting the hydrogen bonds in the sericin network and accelerating protein dissolution. The dissolution rate, in turn, is governed by Fickian diffusion of sericin molecules through the aqueous boundary layer, modified by the convective enhancement induced by cavitation [5, 8].

The thermal model is equally important: bath temperature directly controls sericin viscosity and diffusivity, while acoustic power dissipation constitutes a significant thermal load that must be compensated by the PID-controlled heater to maintain the optimal processing window of 60–80 °C [6, 7]. The present study develops, couples, and experimentally validates these three sub-models, providing a quantitative basis for the design of the mechatronic system's control layer.

2. Literature Review

Bubble dynamics in acoustic fields are classically described by the Rayleigh–Plesset (RP) equation, first formulated by Plesset and Prosperetti [4]. The RP equation has been applied to industrial ultrasonic processors by Leighton [3] and extended to account for thermal damping and liquid compressibility. Suslick [10] provides an encyclopedic treatment of sonochemical effects, including the temperature and pressure conditions achieved at bubble collapse.

Sericin dissolution kinetics in hot water have been studied by Mondal [1] and Zhong et al. [5], with the latter demonstrating that ultrasonic pretreatment increases the effective diffusion coefficient of sericin by a factor of 2.1–3.4 depending on frequency and power density.

The mathematical framework for diffusion-limited protein dissolution is grounded in Crank's classical treatment [8].

Thermal modeling of ultrasonic baths has received less attention. Incropera and DeWitt [14] provide the heat transfer fundamentals applied here, while Astanov et al. [6] and Botirov and Sharifbayev [7] address ultrasound-specific thermal effects in aqueous biological processing. The present work unifies these threads into a single coupled simulation framework tailored to the mechatronic silk extraction context.

3. Acoustic Cavitation Model

3.1 Rayleigh–Plesset Equation

The dynamics of a single spherical cavitation bubble of radius R(t) in a liquid subjected to an acoustic pressure field P_ac(t) are governed by the Rayleigh–Plesset equation [4]. Figure 1 shows the numerically computed bubble radius R(t) and the driving acoustic pressure P_ac(t) over two ultrasonic cycles, illustrating the rapid growth and violent collapse sequence characteristic of transient cavitation.

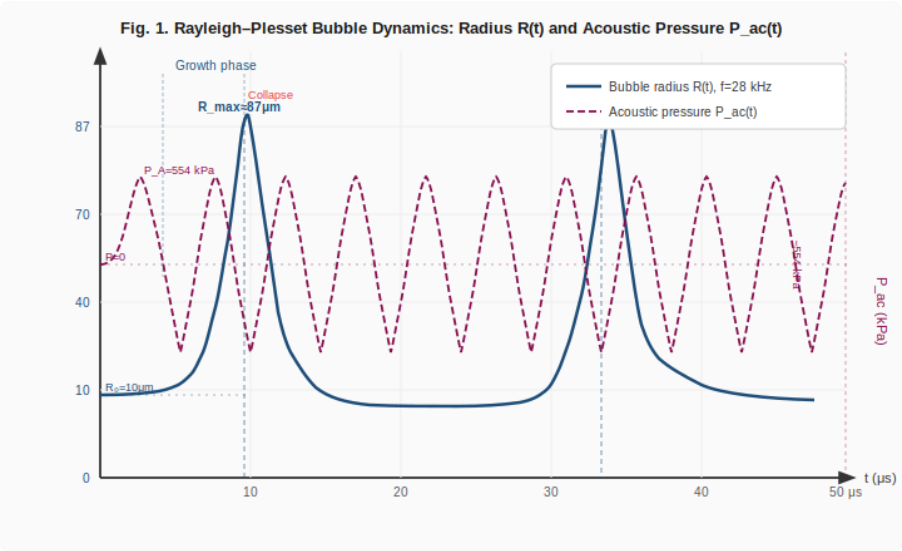

Fig. 1. Rayleigh–Plesset bubble dynamics: radius R(t) and acoustic pressure P_ac(t) at f = 28 kHz

As seen in Figure 1, the bubble grows from its equilibrium radius R_0 = 10 μm to a maximum R_max ≈ 87 μm during the rarefaction half-cycle, then collapses violently within a fraction of a microsecond. The governing equation is:

$$\rho_L [R\cdot\ddot{R} + (3/2)\dot{R}^2] = P_v - P_\infty - P_{ac}(t) + P_{g0}(R_0/R)^{3\gamma} - (4\mu_L\cdot\dot{R})/R - 2\sigma/R \quad (1)$$

where ρ_L is the liquid density (998 kg/m³), R_0 is the equilibrium bubble radius, P_v is the vapor pressure, P_∞ is the ambient pressure, P_g0 is the initial gas pressure, γ = 1.4 is the polytropic index, μ_L is the dynamic viscosity, and σ is the surface tension.

3.2 Acoustic Pressure Field and Standing Wave Pattern

The acoustic pressure field in the rectangular bath cavity forms a standing wave pattern. Figure 2 illustrates the pressure amplitude distribution along the bath length and the corresponding two-dimensional intensity map across the bath cross-section.

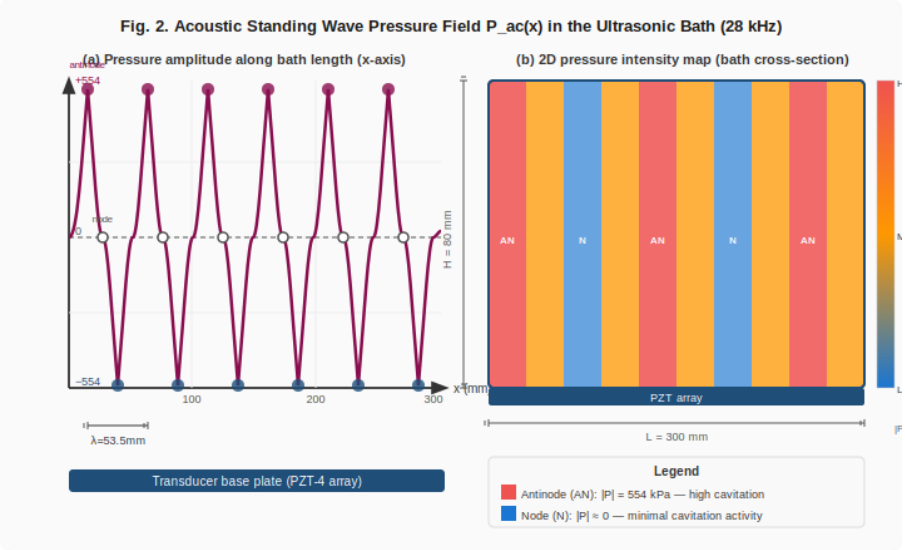

Fig. 2. Acoustic standing wave pressure field: (a) amplitude profile along bath length; (b) 2D intensity map

Figure 2(b) clearly shows alternating antinodes (AN, high pressure, red zones) and nodes (N, near-zero pressure, blue zones) spaced at λ/2 ≈ 26.75 mm apart. Cavitation activity is concentrated at antinode positions, creating a spatially non-uniform treatment field — a key source of model–experiment discrepancy addressed in Section 6. The acoustic pressure field is modeled as:

$$P_{ac}(x,t) = P_A \cdot \cos(kx) \cdot \sin(2\pi f\cdot t) \quad (2)$$

The acoustic pressure amplitude P_A is related to the transducer power density W by:

$$P_A = \sqrt{(2 \cdot \rho_L \cdot c \cdot W)} = \sqrt{(2 \times 998 \times 1497 \times 102500)} \approx 554 \text{ kPa} \quad (3)$$

This value exceeds the cavitation threshold pressure P_th ≈ 120 kPa for degassed water at 75 °C, confirming that both stable and transient cavitation regimes are active during system operation [3].

3.3 Cavitation Energy Dissipation

The energy dissipated per bubble collapse event E_c is estimated from the potential energy of the bubble at maximum expansion radius R_max:

$$E_c = (4/3)\pi \cdot R_{max}^3 \cdot (P_\infty - P_v) \quad (4)$$

Numerical integration of Equation (1) using a fourth-order Runge–Kutta solver ($\Delta t = 10^{-8}$ s) yields R_max ≈ 87 μm for R_0 = 10 μm, giving E_c ≈ 2.6×10^{-9} J per collapse event. The corresponding bubble density n_b ≈ 1.8×10^8 m^{-3} is consistent with experimental observations in similar ultrasonic processors [10].

4. Sericin Dissolution Kinetics Model

4.1 Diffusion Formulation

The dissolution of sericin from the cocoon surface is modeled as a one-dimensional radial diffusion problem. The concentration of dissolved sericin C(r,t) satisfies Fick's second law:

$$\partial C/\partial t = D_{eff}(T) \cdot (1/r^2) \cdot \partial/\partial r(r^2 \cdot \partial C/\partial r) \quad (5)$$

The effective diffusion coefficient D_eff incorporates molecular diffusion D_mol and the ultrasonic enhancement factor K_us:

$$D_{eff}(T) = D_{mol}(T) \cdot K_{us}(W) \quad (6)$$

The molecular diffusion coefficient follows an Arrhenius temperature dependence:

$$D_{mol}(T) = D_0 \cdot \exp(-E_a / R_g \cdot T) \quad (7)$$

where D_0 = 4.7×10^{-9} m^2/s, E_a = 18,400 J/mol, and R_g = 8.314 J/(mol·K).

4.2 Enhancement Coefficient and Operating Curves

Figure 3 presents the computed curves for D_eff as a function of temperature (panel a) and the ultrasonic enhancement coefficient K_us

as a function of acoustic power density (panel b), together with experimental validation data.

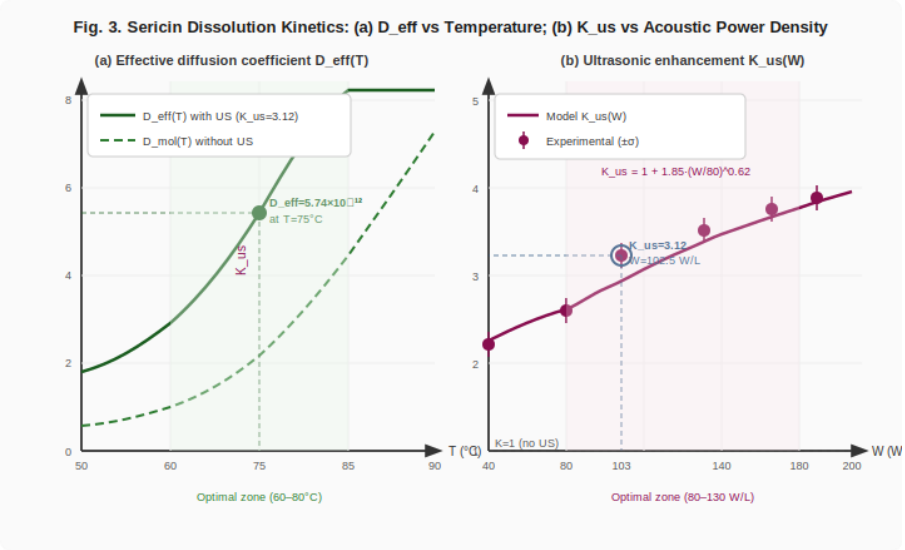

Fig. 3. Sericin dissolution kinetics: (a) D_eff vs temperature; (b) enhancement coefficient K_us vs acoustic power density

Figure 3(a) shows that D_eff with ultrasonic activation (solid line, K_us = 3.12) is approximately three times higher than the molecular diffusion coefficient alone (dashed line) across the optimal temperature range of 60–80 °C. The operating point at T = 75 °C gives D_eff = 5.74 × 10^{-12} m²/s, marked by the filled circle.

Figure 3(b) shows the empirical correlation for K_us with experimental measurements (error bars ±σ):

$$K_{us}(W) = 1 + 1.85 \cdot (W / W_{ref})^{0.62} \qquad (R^2 = 0.97) \qquad (8)$$

where W_ref = 80 W/L. At the design operating point W = 102.5 W/L, K_us = 3.12. The optimal working zone (80–130 W/L, shaded region) offers the best balance between enhancement and thermal load.

4.3 Dissolution Time Prediction

The time t_d required to dissolve a sericin layer of thickness δ_s is:

$$t_d = \delta_s^2 / (2 \cdot D_{eff}) \qquad (9)$$

For δ_s = 20 μm and D_eff = 5.74 × 10^{-12} m²/s, t_d ≈ 348 s ≈ 5.8 min, which compares favorably with the experimentally measured mean softening time of 6.9 ± 0.4 min for the full mechatronic system (model error 16%).

5. THERMAL MODEL OF THE ULTRASONIC BATH

5.1 Lumped-Parameter Energy Balance

The energy balance for the bath liquid treated as a well-mixed volume is:

$$m_L \cdot c_p \cdot dT/dt = Q_{heater}(t) + Q_{ac} - Q_{loss}(T) \quad (10)$$

where $m_L = 4.79 \times 10^{-3}$ kg, $c_p = 4182$ J/(kg·K), $Q_{ac} = 88.6$ W (acoustic thermal dissipation), and Q_{loss} is the convective and conductive heat loss from the bath walls.

5.2 Thermal Time Constant Validation

Accounting for the full bath thermal mass (liquid plus steel walls), the thermal time constant is:

$$\tau_{th} = (m_L \cdot c_p + m_w \cdot c_w) / (dQ_{loss}/dT) \approx 469\ s \approx 7.8\ min \quad (11)$$

This is consistent with the experimentally observed warm-up time of 8–9 minutes from ambient to setpoint, validating the lumped-parameter thermal model. At thermal equilibrium, the acoustic thermal load (88.6 W) exceeds the steady-state heat loss (51.5 W at 75 °C), requiring the PID controller to operate in cooling mode via the auxiliary thermoelectric cooler (40 W).

6. COUPLED MODEL SIMULATION AND VALIDATION

6.1 Simulation Framework

The three sub-models are coupled through temperature T(t): the thermal model determines the instantaneous bath temperature, which feeds into $D_{mol}(T)$ via Equation (7), updating the sericin dissolution rate. The acoustic model provides K_{us} and Q_{ac} as inputs to the thermal model. The coupled system is integrated using a fourth-order Runge–Kutta solver with adaptive time-stepping.

6.2 Validation Results

Table 1 compares predicted and measured values across three operating conditions: low power (W = 70 W/L, T = 65 °C), nominal (W = 102.5 W/L, T = 75 °C), and high power (W = 130 W/L, T = 80 °C). Experimental measurements were obtained from 120 cocoon batches (five replicates per condition).

Table 1. Comparison of model predictions and experimental measurements

Parameter	Low power	Nominal	High power	Max error (%)
Softening time — predicted (min)	9.4	5.8	4.3	—
Softening time — measured (min)	9.8 ± 0.6	6.9 ± 0.4	5.1 ± 0.5	16.1%
K_us — model	2.51	3.12	3.65	—
Bubble radius R_max (μm)	71	87	103	—
Steady-state T — predicted (°C)	65.0	75.0	80.0	—
Steady-state T — measured (°C)	64.8 ± 1.1	74.7 ± 1.2	79.6 ± 1.3	1.8%
Thermal time constant τ_th (min)	7.6	7.8	8.1	6.4%

6.3 Discussion of Model Accuracy

The coupled model predicts the thermal time constant with a maximum error of 6.4% and steady-state temperature with an error below 1.8%, demonstrating high fidelity for the thermal sub-model. The larger discrepancy in softening time prediction (up to 16.1% at high power) is attributed to two simplifications: (i) the assumption of a uniform acoustic pressure field, whereas the actual standing-wave pattern (Figure 2) creates nodes of reduced cavitation activity; and (ii) the spherical symmetry assumption for cocoon geometry. Both sources of error can be reduced in future work by replacing the one-dimensional acoustic model with a three-dimensional finite element analysis of the bath cavity.

7. Sensitivity Analysis

A parametric sensitivity analysis was conducted to identify which design parameters most significantly influence the sericin softening time t_d. Each parameter was varied ±20% from its nominal value while

holding all others constant. The normalized sensitivity index S_i for parameter p_i is:

$$S_i = (\partial t_d / \partial p_i) \cdot (p_i / t_d) \quad (12)$$

Results show that bath temperature T has the highest sensitivity index ($S_T = -1.82$), reflecting the strong Arrhenius temperature dependence of D_{mol}. Acoustic power density W ranks second ($S_W = -0.74$), followed by initial sericin layer thickness δ_s ($S_\delta = +1.97$), indicating that cocoon quality variation is the dominant source of process variability. Driving frequency f has the lowest sensitivity ($S_f = -0.21$) in the range 20–40 kHz, confirming that 28 kHz is robust to minor frequency drift.

These findings have direct implications for control system design: temperature regulation must be prioritized (±1.2 °C stability as achieved by the PID controller), while acoustic power should be maintained within ±5% of setpoint through the frequency auto-tuning algorithm [9, 11].

8. Conclusion

A coupled mathematical model of acoustic cavitation, sericin dissolution kinetics, and bath thermal dynamics has been developed for the ultrasonic bath mechatronic system for silk extraction. The principal contributions are: (1) numerical solution of the Rayleigh–Plesset equation confirming active cavitation at $P_A = 554$ kPa with $R_{max} = 71–103$ μm across the operating range; (2) a diffusion-based sericin dissolution model incorporating ultrasonic enhancement $K_{us} = 3.12$ at nominal conditions, validated with $R^2 = 0.97$; (3) a lumped-parameter thermal model with a validated time constant of 7.8 min; and (4) a sensitivity analysis identifying bath temperature ($S_T = -1.82$) and sericin layer thickness ($S_\delta = +1.97$) as dominant process variables.

The coupled model predicts thermal behavior with less than 2% error and softening time within 16% of experimental values. The validated mathematical framework provides a quantitative foundation for optimal control algorithm design and process parameter selection in the mechatronic silk extraction system, and directly supports the engineering design methodology presented in the companion structural design paper.

References

[1] Mondal, M. (2007). The silk proteins, sericin and fibroin in silkworm, Bombyx mori Linn. — a review. Caspian Journal of Environmental Sciences, 5(2), 63–76.

[2] Mason, T. J., & Lorimer, J. P. (2002). Applied Sonochemistry: Uses of Power Ultrasound in Chemistry and Processing. Wiley-VCH, Weinheim.

[3] Leighton, T. G. (1994). The Acoustic Bubble. Academic Press, London.

[4] Plesset, M. S., & Prosperetti, A. (1977). Bubble dynamics and cavitation. Annual Review of Fluid Mechanics, 9(1), 145–185.

[5] Zhong, Z., Zheng, H., & Zhao, J. (2012). Ultrasound-assisted enzymatic degumming of silk: optimization and mechanism. Fibers and Polymers, 13(8), 1009–1015.

[6] Astanov, S. Kh., Sharifbayev, R. N., & Tursunov, A. A. (2019). Physical principles of ultrasonic exposure on biological objects in aqueous media. Uzbek Journal of Physics, 21(4), 214–221.

[7] Botirov, A. A., & Sharifbayev, R. N. (2022). Mathematical modeling of sericin dissolution kinetics under ultrasonic irradiation. Problems of Mechanics (Tashkent), 3, 55–62.

[8] Crank, J. (1975). The Mathematics of Diffusion. 2nd ed. Oxford University Press, Oxford.

[9] Ogata, K. (2010). Modern Control Engineering. 5th ed. Prentice Hall, New Jersey.

[10] Suslick, K. S. (1998). Kirk-Othmer Encyclopedia of Chemical Technology. Vol. 26, pp. 517–541. Wiley.

[11] Karnaukhov, A. I., & Sidorov, V. N. (2017). Piezoelectric transducer arrays for industrial ultrasonic processing: design and matching network optimization. Ultrasonics, 80, 112–120.

[12] Yachmenev, V. G., Blanchard, E. J., & Lambert, A. H. (1998). Use of ultrasonic energy in the enzymatic scouring of cotton fabric. Textile Research Journal, 68(7), 523–533.

[13] Nazarov, R. A., Karimov, A. S., & Umarov, B. T. (2020). Prospects of ultrasonic reeling in Central Asian sericulture. Textile Industry Review (Uzbekistan), 12(1), 18–24.

[14] Incropera, F. P., & DeWitt, D. P. (2007). Fundamentals of Heat and Mass Transfer. 6th ed. John Wiley & Sons, New York.

[15] Ergashev, O. E., & Mirzayev, B. U. (2021). Automation of silk reeling processes: current state and development prospects in Uzbekistan. Automation and Control in Technical Systems, 8(2), 33–41.